Removal of Hydrogen Sulfide from a Fuel Gas Stream by Electrochemical Membrane Separation

Alan Burke,[a,*,z] Jack Winnick,[a,] Changrong Xia,[b] and Meilin Liu[b,**]**

[a]School of Chemical Engineering and [b]School of Material Science and Engineering, Georgia Institute of Technology, Atlanta, Georgia 30332, USA

A laboratory-scale electrochemical cell was used for desulfurization of a synthetic fuel gas process stream containing up to 3000 ppm H_2S. The cell was run at typical gasifier temperatures (600-650°C) and ambient pressure. The removal rate of H_2S can be limited either by gaseous diffusion from the fuel stream to the cathode-electrolyte interface or by liquid diffusion of sulfur ions through the electrolytic membrane, depending on operating conditions (*i.e.*, temperature and H_2S concentration) and cell design (such as membrane thickness, membrane tortuosity, and flow channel design). For a 200 mL/min gas flow with a composition of 34.14% CO, 22.16% CO_2, 35.13% H_2, 8.51% H_2O, and 1200 ppm H_2S at 600°C, the rate of H_2S removal was determined to be limited by diffusion of sulfide ions through a porous membrane with a thickness of 0.9 mm, a porosity of 38%, and a tortuosity of 3.8. The cell achieved removal fluxes on the order of 1.1×10^{-6} g mol H_2S min^{-1} cm^{-2} at 650°C. While $Y_{0.9}Ca_{0.1}FeO_3$ cathode offered adequate stability and conductivity to study the system at temperatures up to 700°C, the long-term cathode stability is still under investigation.
© 2002 The Electrochemical Society. [DOI: 10.1149/1.1511190] All rights reserved.

H_2S removal.—Hydrogen sulfide is a corrosive contaminant in coal gasification and diesel fuel reformate streams, and it must be removed to make each fuel a viable energy source. Representative compositions vary extensively for each process stream; examples are shown in Table I. In cases where combustion turbines are used, H_2S levels of 100 ppm are permissible. However, for most fuel cell applications, H_2S levels must be lowered below 1 ppm to avoid degradation of cell components.

Fuel gas processes operate from 550 to 2000°C at 1-35 bar. At present, low temperature absorption processes and Claus plants are used to remove sulfur and salvage it as a salable by-product. These removal procedures can often be as extensive as the rest of the process.[1] High temperature absorption processes offer an energy-efficient route for dry fuel streams, but the regeneration of the metal-oxide sorbent is an expensive and difficult process. In addition, the high flow rates of fuel processing (on the order of 7000 lb/day) dictate that vast amounts of sorbent would have to be used and then treated.[2]

To compete with these processes, a high-temperature electrochemical membrane separation has been proposed to remove H_2S in one continuous step, polishing the fuel gas stream while extracting elemental sulfur.[3] Such a process would negate the need for both catalyst regeneration and reheating. The theoretical basis of this separation is an extension of membrane separations driven by pressure gradients. The difference here is that an electric potential, $\Delta\Phi$, is also used to drive species across the membrane, thus adding to the chemical potential to attain the difference in electrochemical potential for species i, $\Delta\overline{\mu_i}$

$$\Delta\overline{\mu_i} = RT \ln(a_i/a_i') + z_i F \Delta\Phi_{(i-i')} \quad [1]$$

a_i and a_i' are the respective activities of component i on either side of the membrane (with ′ indicating the extract phase), z_i is the charge of the transferred species, R is the ideal gas constant, T is the temperature, and F is Faraday's constant.

Steps in H_2S electrochemical removal.—In electrochemical removal of H_2S, the basic steps are (*i*) gaseous diffusion of H_2S to the electrode, (*ii*) H_2S diffusion through the electrode pores to the electrolyte-electrode interface, (*iii*) adsorption and reduction of H_2S at the cathode surface, producing a sulfide ion (S^{2-}), (*iv*) migration and diffusion of sulfide ions through the electrolytic membrane, (*v*) oxidation of S^{2-} to elemental sulfur at the anode, (*vi*) desorption of sulfur at the anode, and (*vii*) diffusion of sulfur away into the bulk purge stream. Previous studies have shown that the reaction kinetics at both the cathode and anode are rapid enough (~ 0.1 A/cm^2) to be negligible in determining the rate-limiting step.[4,5] One aspect of this research has been focused on the first and fourth steps, which must be characterized for each system to determine which is the rate-limiting step as they are both dependent upon temperature, H_2S inlet concentration, and cell design. The preferable reactions are shown below
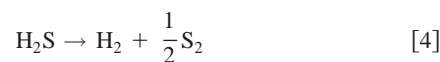
At the cathode

$$2e^- + H_2S \rightarrow H_2 + S^{2-} \quad [2]$$

At the anode

$$S^{2-} \rightarrow \frac{1}{2}S_2 + 2e^- \quad [3]$$
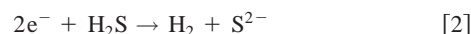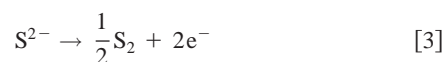
resulting in the net reaction below in which $E° = -0.245$ V at 600°C

$$H_2S \rightarrow H_2 + \frac{1}{2}S_2 \quad [4]$$

Therefore, if H_2S is considered to be the only electroactive species, the necessary applied current can be calculated according to the limitations set on its diffusive and migratory capabilities.

Electrochemical cell components.—The electrolytic cell has five basic components as shown in Fig. 1; cell housing, an inert ceramic membrane, a molten electrolyte, an anode, and a cathode. The cell housing provides the channel medium by which the fuel and purge gas streams flow across their respective electrode surfaces. A metallic cell housing may also act as a current collector to which metal leads can be attached.

The inert, porous ceramic membrane holds the molten electrolyte within its porous structure to create a barrier between the two gas streams and electrodes. Lithiated alumina and yttria-stabilized zirconia (YSZ) have each been popular choices because of their resistance to high bubble pressure as well as inertness and stability in molten carbonate. YSZ is used in this research because it performs well with sulfide present.

Table I. Typical molar component percentages of coal gasification and diesel reformate streams.

Component	Oxygen-blown coal gasification stream (mol %)	Diesel reformate stream (mol %)
CO	30-45	10-25
CO_2	5-25	10-25
H_2O	0-12	10-25
H_2	20-35	40-60
H_2S	Up to 5	Up to 2

The electrolyte in this system must be liquid at the operating temperature, allowing sulfide species to form, and must be stable and conductive while exposed to the sour fuel gas and high temperature. The molten carbonate fuel cell (MCFC) electrolyte, $(Li_{0.62}K_{0.38})CO_3$, was chosen for this work as it satisfies these criteria.

The anode material of lithiated NiO has been selected because it is the predicted stable phase under operating conditions, as shown by Ingram and Janz.[6] It has performed adequately in all runs by maintaining stability in the oxidizing environment.

Cathode material.—With the applied current being so low (less than 0.1 A cm^{-2}) and the electrochemical reaction rate on the order of 0.1 A cm^{-2}, a material with an electrical conductivity of 15 S cm^{-1} should minimize ohmic loss (taking the electrode thickness to be 1 mm). Nickel works well; however, upon conversion to Ni_3S_2, its melting point decreases to 635°C, limiting the range of operation to relatively low temperatures. When inlet H_2S levels are below 60 ppm in polishing applications, nickel has shown promise probably by avoiding formation of nickel sulfide.[7,8]

Other materials have been tested in the search for a more flexible cathode. Lithiated $Y_{0.9}Ca_{0.1}FeO_3$ was shown to be stable and conductive under various operating conditions.[9] CoS_2 has also been predicted to be stable and preferentially convert to Co_9S_8 under process conditions.[10] These materials were used in this study to gather H_2S removal data under various operating conditions.

Theory

Sulfide diffusion limitation across the membrane.—The limiting current density carried by sulfide ions, which is equivalent to the maximum H_2S removal flux, can be estimated from the sulfide diffusion rate across the membrane

$$Flux = \frac{i_{diff}}{nF} = D_{S^{2-}-Elec} \frac{\varepsilon \rho_{Elec}}{\tau} \frac{c_{S^{2-}}^{cath}}{x} \qquad [5]$$

where n is the number of electrons transferred per mole reacted (2 mol^{-1} in this reaction), ε the porosity of the membrane, τ membrane tortuosity, ρ_{Elec} electrolyte molar density in mol cm^{-3}, x membrane
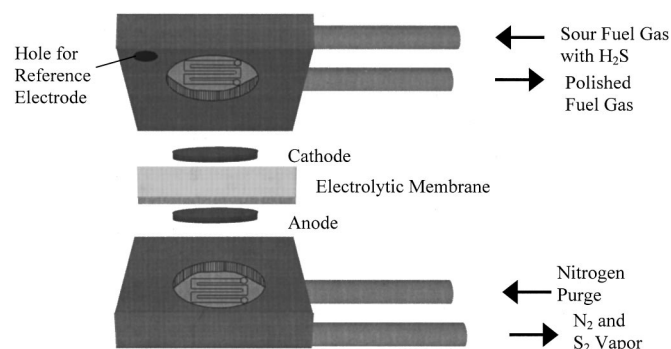
Figure 1. Bench-scale design of electrolytic cell.

thickness in cm, and $D_{S^{2-}/Elec}$ the diffusivity of sulfur ions in the electrolyte (10^{-5} cm^2 s^{-1}).[11] Equation 5 results from consideration of the diffusive flux of sulfide ions through the membrane. Any contribution to this flux by migration is assumed to be negligible due to the presence of supporting electrolyte, alkali carbonate. Other key assumptions are that the activity coefficients of carbonate and sulfide are equal, the mole fraction of sulfide species at the cathode, $c_{S^-}^{cath}$, is at the thermodynamic equilibrium percentage for that temperature, and the concentration of sulfide at the anode is zero. The quantity, $c_{S^-}^{cath}$, is calculated from the equilibrium ratio of Reaction 6, with $[H_2S]$ being the log-mean bulk concentration of H_2S in the cathode gas

$$(Li_{0.62}K_{0.38})_2CO_3 + H_2S \rightarrow (Li_{0.62}K_{0.38})_2S + CO_2 + H_2O \qquad [6]$$
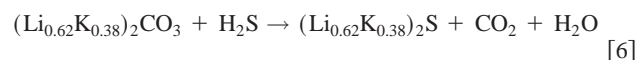
Also, the concentration profiles of carbonate and sulfide across the membrane are assumed to be linear. All parameters in Eq. 5 except τ are independently evaluated.

Gas mass transport limitations.—Mass transfer of H_2S from the process gas to the electrode-electrolyte interface could also be a rate-limiting factor. The mass-transfer coefficient, k_m, can be estimated using Sherwood number correlations based upon rectangular channels in laminar flow regimes.[12,13] The log-mean average offers the most accurate estimate of the average H_2S concentration present. The inlet and outlet mole fractions of H_2S are y_{inlet} and y_{outlet}, and ρ_{fg} is the fuel gas molar density

$$i_{mt} = nFk_m\rho_{fg} \frac{(y_{inlet} - y_{outlet})}{\ln(y_{inlet}/y_{outlet})} \qquad [7]$$

Stoichiometric limitations.—Finally, the stoichiometric limiting current is determined by Faraday's law. For example, if H_2S is the only electroactive species, then the current given below is the minimum needed to remove all inlet H_2S

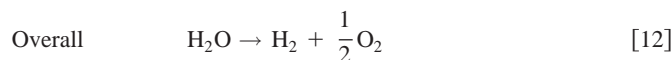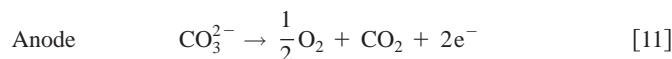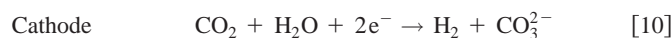$$i_{theo}A = nF\dot{n}_{H_2S} \approx nF \frac{P\dot{V}}{RT} y_{inlet,H_2S} \qquad [8]$$

For instance, if the fuel gas flow rate is 100 cm^3 min^{-1} and the inlet H_2S concentration is 1000 ppm, then the maximum i_{theo} that can be passed by sulfur ions is 1.69 mA cm^{-2}.

If other reactions occur, then higher currents will have to be applied and the H_2S removal current efficiency will decrease. One concern is microcracking in the membrane, which could allow H_2 to diffuse to the other side. If hydrogen is present at the anode, then the parasitic reaction below will take place

$$H_2 + CO_3^{2-} \rightarrow H_2O + CO_2 + 2e^- \qquad [9]$$

Pressure gradients may also drive Reaction 9 by pushing H_2 through the membrane.

Nernstian effects.—In another parasitic process, Reactions 10 and 11 below combine to yield Reaction 12; carbon dioxide is transported across the cell as water is electrolyzed

Cathode $\qquad CO_2 + H_2O + 2e^- \rightarrow H_2 + CO_3^{2-} \qquad [10]$

Anode $\qquad CO_3^{2-} \rightarrow \frac{1}{2}O_2 + CO_2 + 2e^- \qquad [11]$

Overall $\qquad H_2O \rightarrow H_2 + \frac{1}{2}O_2 \qquad [12]$

The actual cell potential, E, may deviate from the standard potential, $E°$, because of concentration (activity) differences at each

electrode as shown in Eq. 13 and 14. Additionally, taking E to be equivalent for both sets of reactions, one can estimate the relative extent of each reaction

$$E = E_4^0 - \frac{RT}{nF} \left\{ \ln \left[\frac{(p_{S_2})^{1/2}}{a_{S^{2-}}} \right]_{anode} + \ln \left[\frac{p_{H_2} a_{S^{2-}}}{p_{H_2S}} \right]_{cathode} \right\} \quad [13]$$

$$E = E_{11}^0 - \frac{RT}{nF} \left\{ \ln \left[\frac{p_{CO_2}(p_{O_2})^{1/2}}{a_{CO_3^{2-}}} \right]_{anode} + \ln \left[\frac{p_{H_2} a_{CO_3^{2-}}}{p_{CO_2} p_{H_2O}} \right]_{cathode} \right\}$$

$$[14]$$

For instance, at 600°C and 1 atm, the standard potentials for Reactions 4 and 12 are $E_4^0 = -0.245$ V and $E_{12}^0 = -1.04$ V (thus H_2S dissociation is favored). Given the typical gas stream tested, the cathode side molar composition is 35.1% H_2, 22.2% CO_2, and 8.5% H_2O with a log-mean average of 1000 ppm H_2S. With the sum of liquid-phase activities at the cathode being unity, thermodynamic data for Reaction 6 were used to estimate mole fractions of 0.964 and 0.036 for carbonate and sulfide, respectively (assuming activity coefficients are equal to one). On the anode side, the activity of sulfide ions approaches zero while that of the carbonate ion approaches one.

Next, an operating cell potential, E, must be chosen to calculate the CO_2 present at the anode from Eq. 14. This potential is free of ohmic and other non-Nernstian overpotentials. With $E = -0.75$ V, a value common when trying to achieve maximum H_2S removal, an average CO_2 mole percentage of 0.1% exists at the anode (oxygen would then have half of this value).

Finally, setting an anode-side sulfur level allows one to determine the sulfide activity at the anode from Eq. 13. Under these operation conditions, experimental removal data suggest that a log-mean average sulfur level at the anode would be approximately 100 ppm. For this value and the same E value of -0.75 V, the carbonate/sulfide activity ratio in the anolyte is on the order of 10^6. Therefore, a significant sulfide concentration gradient exists through the membrane, and the removal current efficiency is about 16% (the percentage of current contributing to H_2S removal).

Experimentally, however, there is more CO_2 transport most likely due to H_2 crossover. Because of this, a lower removal current efficiency is observed (normally 5-10%). However, with the small H_2S concentrations present and the small currents applied, this low efficiency can still generate excellent removal performance without suffering unacceptable power losses.

Limitations of theory.—A key assumption in Eq. 5, 7, and 8 is that sulfur is the only electroactive species. Because some current is lost to CO_2 transport, however, the required applied current is higher than the currents calculated in these equations. In analysis of the system, the current densities in Eq. 5 and 7 are calculated from Eq. 8 using the molar H_2S removal rates seen in experimentation.

By stepping up the current until the H_2S removal rate reaches a maximum, the maximum H_2S removal rate at a certain temperature, inlet H_2S concentration, and flow rate can be found. From this maximum H_2S removal rate, a membrane tortuosity and mass transfer coefficient can be back-calculated from Eq. 5 and 7, respectively. Reproducibility of these values under various operating conditions can help one gain insight as to which process is rate limiting. Also, Eq. 5, 7, and 8 are derived under steady-state conditions. The current must be held after each alteration for several hours to achieve steady state and acquire valid data points.

Previous Studies

In Fig. 2, results from previous studies are compared to a lithiated nickel cathode run from this study. Success was obtained using a Co_9S_8 cathode and a lithiated alumina membrane.[14,15] These data show how increasing the current yields higher removal even when
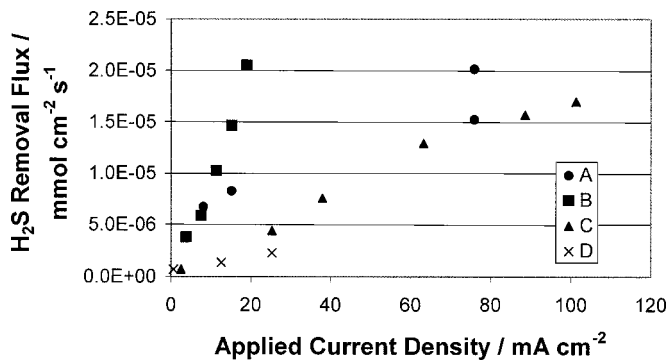
Figure 2. Removal data from previous studies, showing the removal flux of H_2S as current density is stepped upward. Criterion of each run are as follows. (A) $LiY_{0.9}Ca_{0.1}FeO_3$ cathode and prerigidized YSZ membrane (0.9 mm) at 650°C; 3000 ppm H_2S inlet at 100 mL/min.[16] (B) $LiCoO_2$ cathode and prerigidized YSZ membrane (0.6 mm) at 650°C; 3400 ppm H_2S inlet at 100 mL/min.[17] (C) Co_9S_8 cathode and lithiated alumina membrane (1.8 mm) at 650°C; 6500 ppm inlet at 33 mL/min.[14] (D) LiNi cathode and prerigidized YSZ membrane (1.8 mm) at 600°C, 1300 ppm H_2S inlet at 75 mL/min.

the theoretical maximum, i_{theo}, has been surpassed. This occurs because of side reactions, predominately Reactions 10 and 11, exhausting a large portion of applied current due to H_2 crossover and Nernstian effects.

The lithiated nickel run from this study most closely mirrors the Ref. 14 *s* data. Both studies used similar membrane thickness, whereas the Ref. 16 *s* and the Ref. 17 *s* membranes are significantly thinner (0.9 and 0.6 mm, respectively). These data pinpoint membrane thickness as a possible critical factor in achieving maximum H_2S removal rates.
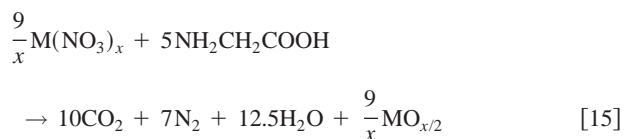
Experimental

Electrode fabrication.—Nickel mesh sheets with 80% porosity were provided by Fuel Cell Energy, Inc. After being cut into 7.9 cm² disks, they were heated in a furnace at 600-800°C for at least 4 h to convert the nickel into nickel oxide. The disk was soaked in 4 M LiOH at room temperature, air dried, and then sanded so that it would fit snugly into the cell housing without protruding into the membrane. This was the anode material for every run.

For the lithiated nickel cathode, the same nickel disks used for the anode were sanded to prevent protrusion into the membrane upon sulfidation. The 7.9 cm² disk was soaked in a solution of 4 M LiOH to lithiate the electrode, and, during heat-up, it was purged with nitrogen before fuel gas exposure to help prevent conversion to nickel oxide.

Cobalt sulfide electrodes were fabricated using tape-casting techniques as described in Ref. 18. For CoS_2, 1.5 g was added to 0.2 g of binder. A 7.9 cm² disk was then pressed by a 3 cm pneumatic die at 4000 psi and sintered at 450°C for 3 h and then at 615°C for 3 more hours. Cooling to room temperature took place at a rate of 2°C min^{-1}. The CoS_2 electrode was converted to Co_9S_8 and Co_4S_3 mixed phase under operating conditions.

For the $Y_{0.9}Ca_{0.1}FeO_3$ cathode, a combustion synthesis was used. Metal nitrates $[Y(NO_3) \cdot 6H_2O, Ca(NO_3)_2, and Fe(NO_3)_3 \cdot 9H_2O]$ and glycine were used to prepare the precursor solution for the combustion synthesis of $Y_{0.9}Ca_{0.1}FeO_3$. Glycine was added in solid form. The glycine-to-nitrate ratio in the precursor solution was set to be 0.60. A stoichiometric mixture of oxidant and fuel might be defined by
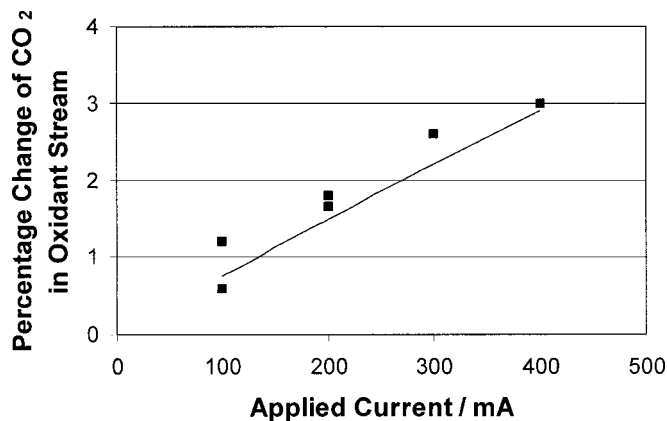
$$\frac{9}{x} M(NO_3)_x + 5NH_2CH_2COOH$$

$$\rightarrow 10CO_2 + 7N_2 + 12.5H_2O + \frac{9}{x} MO_{x/2} \quad [15]$$

Figure 3. CO_2 transport data *vs.* the theoretical rate calculated by Faraday's law.

Figure 4. Equilibrium constants for Reaction 6 calculated from Gibbs free energy via $\Delta G_{rxn} = -R\text{T}\ln(K_{eq})$.

where $x = 2.45$ for the combination of metal nitrates necessary to prepare a product consisting of a mixture of iron oxide, yttrium oxide, and calcium oxide or other phases having the same average metal oxidation state as in the precursor. A stoichiometric oxidant/fuel mixture would thus contain 0.56 glycine molecules per nitrate ion. Combustion of the metal nitrate/glycine solutions was performed in glass beakers on an infrared hot plate, with typically 10 mL of the precursor solution (0.2 mol with respect to iron) burned at a time. The precursors were concentrated by heating until excess free water was evaporated, at which point spontaneous ignition occurred and resulted in black ash. The ash was then calcined at 800°C for 2 h to get $Y_{0.9}Ca_{0.1}FeO_{3-\delta}$. X-ray diffraction (XRD) analysis showed that the powder had orthorhombic structure. Isothermal adsorption/desorption investigation showed that the specific surface area of the powder was 143 m^2g^{-1}, about seven times higher than that for the powder prepared by solid-state reaction (19 m^2g^{-1}). A 3 cm circular die was used for 1 g at 7000 psi. Polyvinyl alcohol was added as binder and starch as pore former. The cathode was sintered at 1000°C for 2 h before using. The porosity of the cathode was 43% as measured by the standard Archimedes method.

Cell housing fabrication and passivation.—Cell housings were fabricated from stainless steel 304 blocks ($2 \times 2 \times 0.75$ in.). A 1 mm deep circular indention was cut for the electrode cavity. A rectangular flow channel was cut into this indention for gas to flow across the electrode. Metal tubing extended from the cell housing to outside of the furnace to make gas flow and circuit connections. Finally, a quarter-inch diameter hole was drilled in an upper corner of the cell housing to be placed on top in order to provide access for a reference electrode to the membrane. The reference gas composition was 15% CO_2, 3% O_2, and the balance N_2, and either a gold or platinum wire touching a corner of the membrane was used as a current collector.

In an attempt to avoid corrosion of the steel cell housing, a thin layer of alumina was layered on its surface, which contacts the membrane but not the electrode. A solution of aluminum hydroxide was applied to the clean surface of the cell housing and then heated (to about 100°C for a few hours) to leave behind a thin alumina layer.

Assembly of cell housing, electrodes, membrane, and electrolyte.—Before heat-up, the cell was assembled as shown in Fig. 1. The cell was heated at a rate of 100°C h^{-1}, and N_2 was supplied to the cathode side to prevent oxidation if needed. A piston, applying 5 psi, was used to compress the materials together after the electrolyte melted at 490°C. At this point, clean fuel gas was supplied to the cathodic side of the cell, and the N_2 purge was switched
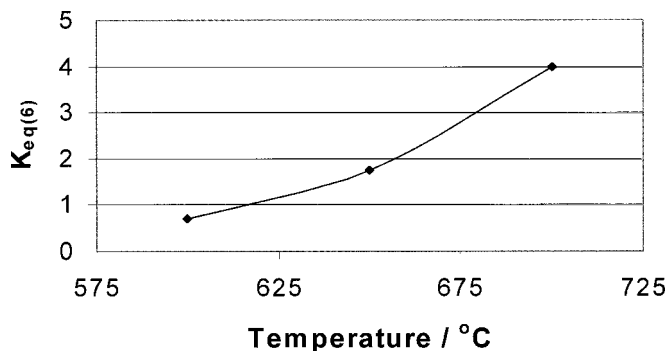
to the anodic side. Flow rates in and out of the cell were checked to verify that there was a good seal between the membrane and cell housings.

After verifying CO_2 transport, a synthetic, sour gas mixture of 36.56% CO, 24.65% CO_2, 38.74% H_2, and 489-2541 ppm H_2S was fed into the system. After passing through a bubbler at 40°C and a shift reactor with Girdler, CCl, and Houdry catalysts, the gas then entered the electrolytic cell. The bubbler was used to mimic hydrated gas streams and to prevent carbon deposition in the reactor via the reaction

$$2CO \rightleftarrows CO_2 + C(s) \qquad [16]$$
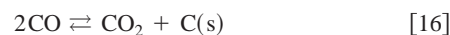
The presence of steam hampers the formation of CO, thus eliminating carbon deposition. Entering the cell, the gas inlet had a composition of 34.14% CO, 22.16% CO_2, 35.13% H_2, 8.51% H_2O, and 450-2500 ppm H_2S at 600°C due to the gas-water shift reaction

$$H_2O + CO \rightleftarrows H_2 + CO_2 \qquad [17]$$

About 2 to 4 days were allotted for the system to reach equilibrium at which point the outlet H_2S concentration reached the inlet concentration. During this time period, the cathode material changed from an oxide to a sulfide compound, and the electrolyte sulfide/carbonate ratio attained equilibrium.

Analytical techniques.—Constant current was applied via a Perkin-Elmer 273A potentiostat/galvanostat. Cells were run at open circuit until the outlet H_2S level reached a magnitude comparable to the inlet. At this point, the cell was operated galvanostatically to initiate electrochemical transfer. Cell resistance was estimated using the current-interrupt method with an oscilloscope. Multimeters were also connected in parallel to the cell to monitor voltages between each electrode and the reference.

Hydrogen sulfide levels were measured using a flame-photometric gas chromatograph (Perkin-Elmer Auto System XL). Gas samples of 60 μL were injected into the column (Chemsorb 102). The temperature of the column was 120°C, and the injection temperature was 250°C. Samples of known concentration were used to calibrate the column, which is accurate within 10% at concentrations above 40 ppm. Cleaning the syringe with ethanol between samples produced the most consistent results.

Infrared spectroscopy was used to monitor the CO_2 levels leaving the anode side. The data were used to verify continued electrochemical activity because CO_2 transport is a side reaction that can be monitored according to Faraday's law.
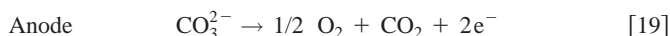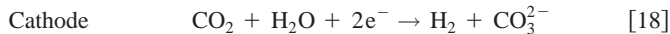
Cathode microstructure and cracking in the ceramic membrane were examined with a Hitachi S-800 scanning electron microscope. XRD was used to determine the crystal structure and phase composition of electrode materials before and after a run.
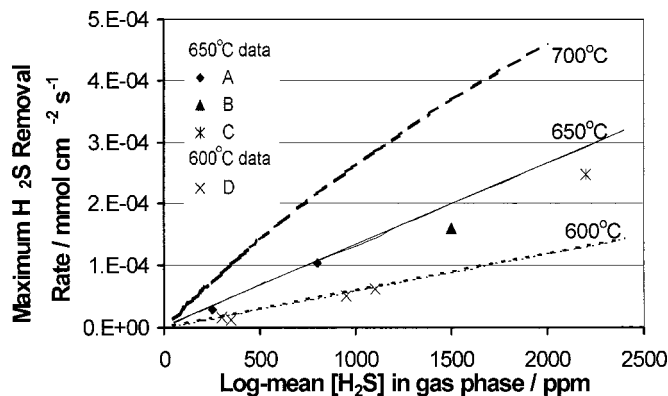
Figure 5. Effect of temperature on H_2S removal rate as a function of log-mean $[H_2S]$. Theoretical plots based upon $x \sim 0.9$ mm, $A = 7.9$ cm^2, and $\tau = 3.6$. (A) $LiY_{0.9}Ca_{0.1}FeO_3$ cathode & prerigidized YSZ membrane (0.9 mm), at 650°C; 500-1000 ppm H_2S inlet at 80 mL/min. (B) $LiY_{0.9}Ca_{0.1}FeO_3$ cathode and prerigidized YSZ membrane (0.9 mm) at 650°C; 3000 ppm H_2S inlet at 100 mL/min[16] (C) $LiCoO_2$ cathode and prerigidized YSZ membrane (0.6 mm) at 650°C; 3400 ppm H_2S inlet at 100 mL/min[17] (D) $LiY_{0.9}Ca_{0.1}FeO_3$ cathode and prerigidized YSZ membrane (0.9 mm) at 600°C; 1300 ppm H_2S inlet at 75 mL/min

Results and Discussion

CO$_2$ transport.—Clean fuel gas was tested first to verify proper functioning of the cell before exposure to H_2S. In a process the reverse to that of a standard MCFC, current is applied to transport CO_2 across the membrane via the reactions

Cathode $\qquad CO_2 + H_2O + 2e^- \rightarrow H_2 + CO_3^{2-} \qquad$ [18]

Anode $\qquad CO_3^{2-} \rightarrow 1/2\ O_2 + CO_2 + 2e^- \qquad$ [19]

The results in Fig. 3 have good stoichiometric agreement with Faraday's law. As the current is stepped upward, more CO_2 is proportionally transported across the membrane.

H$_2$S removal temperature effects.—Following the CO_2 transport experiments, H_2S transport was investigated at two temperatures, 600 and 650°C. The thermodynamic data in Fig. 4 imply that higher H_2S removal rates are possible at higher temperatures because more sulfide is favored in the electrolyte via Reaction 6. This enables more current to go toward sulfur removal because the concentration gradient across the membrane in Eq. 5 will increase (assuming the anode side concentration remains the same, approximately zero). Additionally, higher temperatures generally increase electrode kinetics and diffusivities of species in the electrolyte.
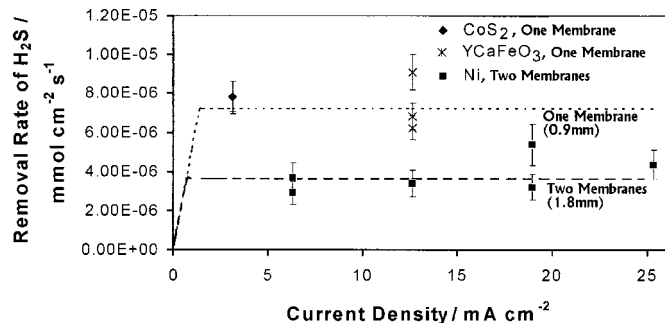
Figure 6. Effect of membrane thickness. Data of two-membrane system *vs.* one-membrane system with specified cathode materials. $T = 600$°C and inlet $[H_2S] = 1200$ppm $\pm$ 50. Fuel gas flow rate was maintained at 200 mL/min. Diffusion-limited plots were calculated using a tortuosity value of 3.6.
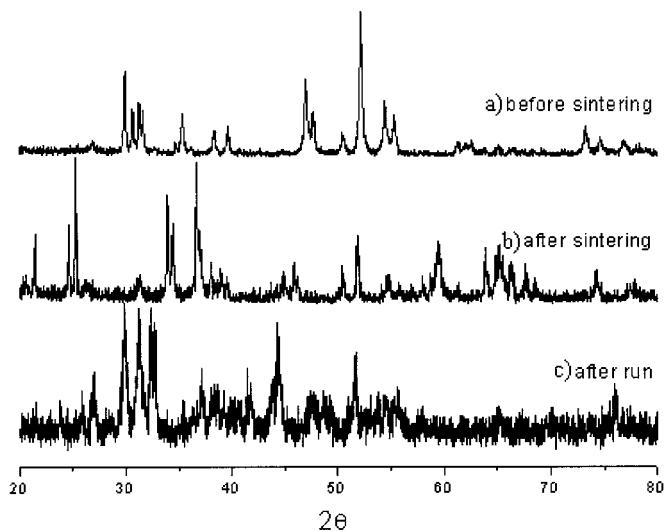
Figure 7. XRD of cobalt sulfide electrode before sintering, after sintering, and after using as a cathode for electrochemical removal of H_2S. The XRD patterns correspond to the following structures: (a) CoS_2, (b) Co_4S_3/Co_3S_4 mixed phase, and (c) Co_9S_8/Co_4S_3 mixed phase.

In Fig. 5, H_2S removal rate depends linearly upon the log-mean average H_2S concentration in the sour gas stream. All of the data are taken from steady-state points at which the current had been ramped to approach the maximum achievable H_2S removal rate. The applied currents used to acquire this data are not shown here for each data point, but each applied current is considerably higher than the theoretical current needed to remove only sulfur because of the interference of side reactions due to CO_2 transport and H_2 crossover.

Comparisons of various data from this and previous studies are shown in Fig. 5. In accordance with theory, data taken from 650°C show higher removal capabilities than those from 600°C. Indeed, higher temperature has only been detrimental to performance when it has led to thermal breakdown of one or more of the cell components.

H$_2$S removal, effect of membrane thickness.—The most convincing evidence supporting membrane diffusion as the limiting process is the comparison of one *vs.* two membranes used in the cell. Equation 5 shows that a membrane twice as thick will decrease the removal rate by half if all other parameters are held constant. By comparing data that vary only by membrane thickness, removal data can be compared to determine whether or not diffusion across the membrane is rate-limiting. The data in Fig. 6 indicate that a membrane half as thick enables about double the removal performance under the given operating conditions.

Each membrane is approximately 0.9 mm thick, so when two membranes are used, the membrane thickness is 1.8 mm. A membrane thickness of 1.8 mm was also used in a previous study,[14] and it should be noted that these data at a higher temperature and H_2S inlet concentration fit with the diffusion-limited theory. In Fig. 2, the applied current was raised to reach an H_2S removal rate of 3.3 mA cm^{-2}, which would be about 26 mA going toward H_2S removal on a 7.9 cm^2 surface, and the log-mean H_2S concentration across the cathode was 2400 ppm. This value, 26 mA, approaches nearly half the value predicted by the 650°C plot in Fig. 5, as it should, because the membrane thickness used is twice that in the plot. Further increase of the current may have led to the maximum removal rate, which would be about 30 mA for these operating conditions as calculated by Eq. 5.

Considering an average data point for a one-membrane system from Fig. 6, the current going toward H_2S removal is 1.31 mA cm^{-2} with the applied current being 12.66 mA cm^{-2}. The applied
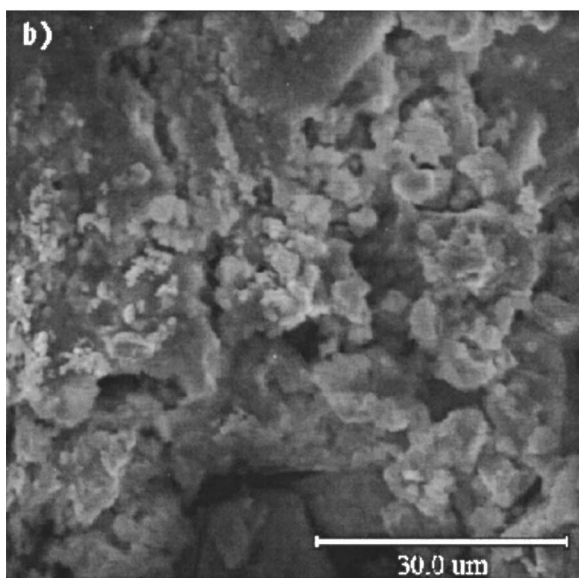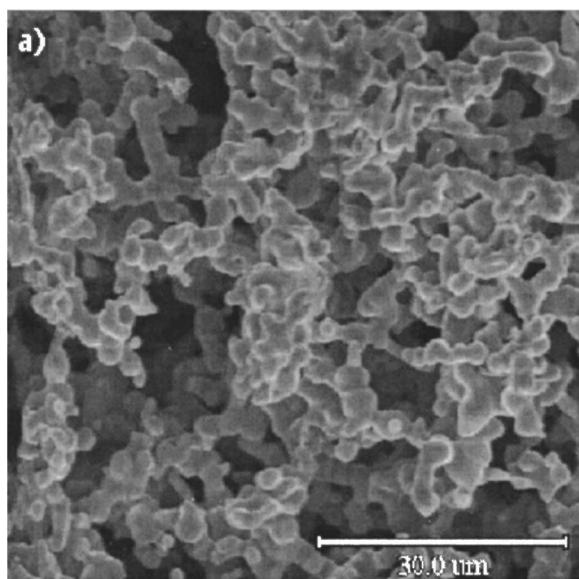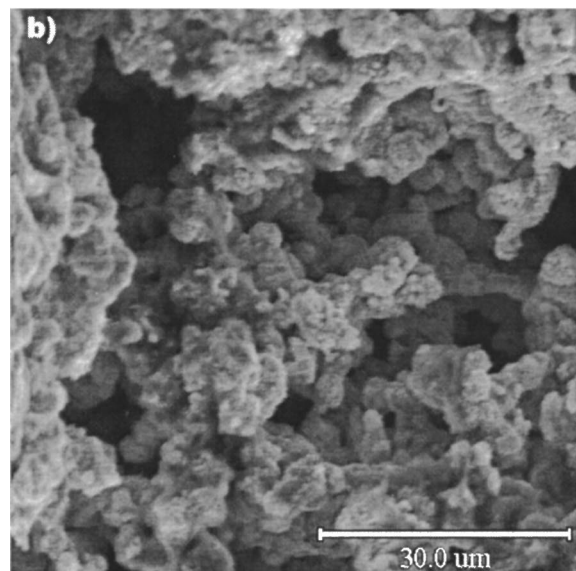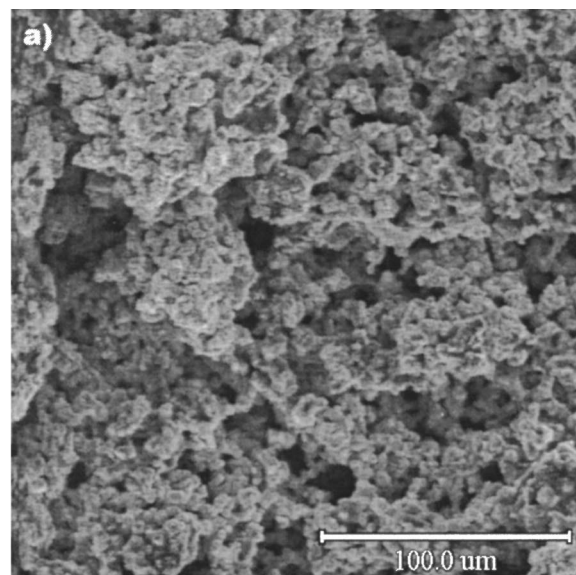
Figure 8. Scanning electron micrograph of nickel cathode before (a) and after (b) run, 1000 times. Notice the clogging of pores after the run.

Figure 9. Scanning electron micrograph of nickel oxide anode after run. Pores appear to be in good condition. (a) 300 times, (b) 1000 times.

current is 332.2% of i_{theo} and results in a molar removal flux of 6.8×10^{-6} mmol of H_2S cm^{-2} s^{-1}. The removal current efficiency here is 10.4%, which is lower than Nernstian relations predict but is consistent from trial to trial. The discrepancy occurs because the Nernstian relation accounts for neither H_2 crossover nor membrane cracks/holes.

In every plot, the effective tortuosity used to fit the data to Eq. 5 is 6, reasonable value for a membrane comprised of submicrometer sized particles. Errors arising from Eq. 5 can be attributed to either a nonlinear activity profile through the membrane and/or sulfur ion levels lower than that of equilibrium in the electrolytic melt caused by formation of polysulfides or other side reactions. Despite supporting evidence, anode sulfide concentration may also be non-zero. Any of these inaccuracies would reduce the concentration gradient, which would reduce the maximum removal rate of H_2S. The tortuosity value could be compensating for any of these possibly erroneous assumptions.

Cathode stability results.—Our results with the cobalt sulfide

electrode were discouraging because the electrode melted during operation. Postmortem XRD analysis showed that the CoS_2 electrode, which had been sintered at 600°C for 4 h to obtain a mixed Co_3S_4/Co_4S_3 phase, had transformed into a mixture of Co_9S_8, which melts at 835°C, and Co_4S_3, which apparently melts below 650°C (see Fig. 7 for XRD analysis). This electrode was very successful in the earlier studies,[14] but, in these studies, the starting material was a single phase of Co_9S_8. Whether or not the Co_9S_8 phase retains its structure throughout various operating conditions (*i.e.*, varied temperature, inlet H_2S concentration, and applied current) remains a question.

The $LiY_{0.9}Ca_{0.1}FeO_3$ cathode also failed after about 150 h, but it was able to run at higher temperatures, thus showing better performance. Our postmortem analysis agreed with Ref. 16, as $LiY_{0.9}Ca_{0.1}FeO_3$ was seen to convert from a metal-oxide semiconductor to a metallic conductor via sulfurization into a Y_2O_2S, FeS mixed phase. The conductivity remains around 15 S cm^{-1} throughout proposed operating temperatures (600-800°C).[8] Higher sintering temperatures (of at least 1000°C) prior to insertion into the cell aids

in stabilizing the microstructure of the cathode, allowing it to endure longer periods of operation.

The nickel cathode material was initially good at 600°C, but failed after about 150 h of operation under H_2S. The industrial grade nickel cathode material had fewer defects than the cathode materials made by hand, so nickel samples were analyzed to ascertain the degradation mechanism at the cathode. The XRD results showed that the nickel cathode was converted, as expected, to a predominantly Ni_3S_2 phase known as heazlewoodite. An extra peak at $2\theta = 63$ offered evidence that the cathode also contained a NiO (bunsenite) phase.

SEM analysis revealed the breakdown of the porous structure in the cathode material (see Fig. 8). A loss of cathode wetting and/or pore size can both result in diminished H_2S gas exposure to the cathode-electrolyte interface. The NiO anode shows no significant sign of damage in Fig. 9 and also no sign of sulfur absorption. This, again, is evidence that the sulfide is oxidizing immediately at the anode; hence, our modeling of the anode sulfide concentration approaching zero is a good approximation.

Finding a suitable cathode material remains the key to further developing the long-term performance of this process. Conductive, sulfur-tolerant materials will continue to be sought out and tested in a full cell. Interest has arisen in strontium-vanadium oxides, Gd_2TiMoO_7, and various cermet materials that have a semiconductive, ceramic matrix impregnated with a conductive metal sulfide.

Conclusions

Experimental results have demonstrated that the diffusion of sulfide ions through the membrane limits the maximum achievable rate of steady-state H_2S removal under the conditions studied. At higher H_2S inlet concentrations or at higher operating temperatures, gaseous diffusion may become the limiting process because a higher sulfide concentration in the electrolyte is favored, allowing for higher membrane diffusion rates. While reducing membrane thickness or increasing its porosity is another avenue for enhancing the sulfide diffusion rate, there are restrictions as to how thin the membrane can be. It must remain thick enough to resist cracking under pressure (from the cell above it) and to prevent excessive H_2 crossover, which can drastically decrease cell efficiency (not to mention the fuel gas calorific value). The exact thickness will ultimately depend upon the specific design of the cell and is still under investigation.

Acknowledgments

List of Symbols

a_i	activity of species i
A	superficial area of electrode, cm^2
c_i	liquid mole fraction of species i, $mol\ mol^{-1}$
D	diffusivity coefficient, $cm^2\ s^{-1}$
$E°$	standard state potential, V
E	actual cross-cell potential, V
F	Faraday's constant, C
i	current density, $A\ cm^{-2}$
K_{eq}	equilibrium constant
k_m	mass transfer coefficient, $cm\ s^{-1}$
M_W	molecular weight, $g\ mol^{-1}$
n	number of equivalents per mole, mol^{-1}
$\dot{n}$	molar flow rate, $mol\ s^{-1}$
p_i	partial pressure of species i, atm
T	temperature, K
$\dot{V}$	volumetric flow rate, $cm^3\ s^{-1}$
x	thickness of membrane, cm
y_i	gaseous mole fraction of species i, $mol\ mol^{-1}$
z_i	molar charge of transferred species i, mol^{-1}

Greek

ε	void volume of membrane
ρ	molar density, $mol\ cm^{-3}$
τ	tortuosity
μ	electrochemical potential, $J\ mol^{-1}$
$\Delta\Phi$	potential drop across membrane, V

Subscripts

elec	electrolyte
fg	fuel gas
diff	diffusion
mt	mass transfer

References

1. P. Nowacki, *Coal Gasification Processes*, p. 326, Noyes Data Corp. Park Ridge, NJ (1981).
2. A. Atimtay and D. Harrison, *Desulfurization of Hot Coal Gas*, p. 91, Springer, Heidelberg (1998).
3. J. Winnick. U.S. Pat. 4,246,081 (1981).
4. M. P. Kang and J. Winnick, *J. Appl. Electrochem.,* **15**, 431 (1985).
5. K. White III and J. Winnick, *Electrochim. Acta,* **30**, 511 (1985).
6. M. D. Ingram and G. J. Janz, *Electrochim. Acta,* **10**, 783 (1965).
7. S. R. Alexander and J. Winnick, *J. Appl. Electrochem.,* **24**, 1092 (1994).
8. S. R. Alexander and J. Winnick, *AIChE J.,* **40**, 613 (1994).
9. S. Wang, M. Liu, and J. Winnick, *J. Solid State Electrochem.,* **5**, 188 (2001).
10. D. Weaver and J. Winnick, *J. Electrochem. Soc.,* **138**, 1626 (1991).
11. E. Majewski and D. Walker, *Earth Planet. Sci. Lett.,* **160**, 823 (1998).
12. J. Robinson and J. Winnick, *J. Appl. Electrochem.,* **28**, 1343 (1998).
13. F. P. Incropera and D. P. DeWitt, *Fundamentals of Heat and Mass Transfer*, 2nd ed., John Wiley & Sons, New York (1987).
14. D. Weaver and J. Winnick, *J. Electrochem. Soc.,* **139**, 492 (1992).
15. D. Weaver and J. Winnick, *J. Electrochem. Soc.,* **134**, 2451 (1987).
16. S. Wang, M. Liu, and J. Winnick, In press.
17. S. Smith, Ph.D. Thesis, Georgia Institute of Technology, Atlanta, GA (1999).
18. J. Niikura, K. Hatoh, N. Taniguchi, T. Gamo, and T. Iwaki, *J. Appl. Electrochem.,* **20**, 606 (1990).